THE JOURNAL OF PHYSICAL CHEMISTRY B

Article

pubs.acs.org/JPCB

Illuminating Photochemistry of an Excitation Ratiometric Fluorescent Protein Calcium Biosensor

Longteng Tang,[†] Yanli Wang,[†] Weimin Liu,[†,§] Yongxin Zhao,[‡,⊥] Robert E. Campbell,[‡] and Chong Fang*[,†]

[†]Department of Chemistry, Oregon State University, Corvallis, Oregon 97331, United States

[‡]Department of Chemistry, University of Alberta, Edmonton, Alberta T6G 2G2, Canada

Supporting Information

ABSTRACT: Fluorescent protein (FP)-based biosensors have become an important and promising tool to track metal ion movement inside living systems. Their working principles after light irradiation, however, remain elusive. To facilitate the rational design of biosensors, we dissect the fluorescence modulation mechanism of a newly developed excitation ratiometric green FP-based Ca^{2+} biosensor, GEX-GECO1, using femtosecond stimulated Raman spectroscopy (FSRS) in the electronic excited state. Upon 400 nm photoexcitation, characteristic vibrational marker bands at ∼1180 and 1300 cm^{-1} show concomitant decay and rise dynamics, probing the progression of an ultrafast excited state proton transfer (ESPT) reaction. The Ca^{2+}-bound biosensor exhibits two distinct populations that undergo ESPT with ∼6 and 80 ps time constants, in contrast to one dominant population with a 25 ps time constant in the Ca^{2+}-free biosensor. This result is supported by key structural constraints from molecular dynamics simulations with and without Ca^{2+}. The blueshift of the ∼1265 cm^{-1} C−O stretch mode unravels the vibrational cooling dynamics of the protonated chromophore regardless of Ca^{2+} binding events. This unique line of inquiry reveals the essential structural dynamics basis of fluorescence modulation inside an excitation ratiometric protein biosensor, correlating the uncovered chromophore structural heterogeneity with different H-bonding configurations and intrinsic proton transfer rate in the photoexcited state.

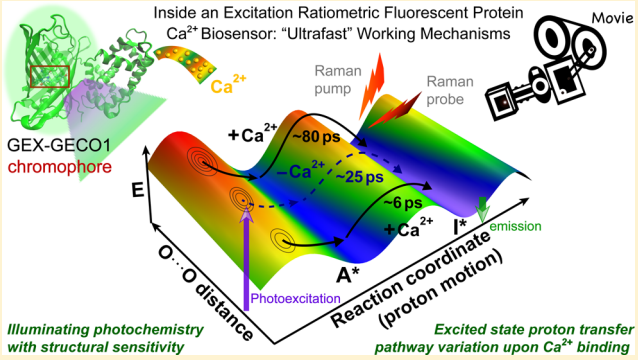

INTRODUCTION

The calcium ion (Ca^{2+}) is one of the most important intracellular second messengers. It plays key roles in regulating numerous cellular processes, including proliferation, fertilization, muscle contraction, neuron firing, disease onset, and progression.[1,2] In order to track Ca^{2+} movement in living systems noninvasively, the fluorescent protein (FP)-based Ca^{2+} biosensors have been developed since the late 1990s because they are genetically encodable and expressable in transgenic organisms.[3−5] Among them, a relatively newcomer GEX-GECO1 is a green excitation ratiometric Ca^{2+} indicator that exhibits a large Ca^{2+}-dependent ratio change (26-fold) with ∼400 and 450 nm light irradiation, and reaches the Ca^{2+}-binding equilibrium faster than the other genetically encoded Ca^{2+} indicators for optical imaging (GECOs).[6] On the molecular level, upon 400 nm photoexcitation, the protonated chromophore of GEX-GECO1 undergoes excited state proton transfer (ESPT) and converts to an intermediate deprotonated form in the electronic excited state that emits green fluorescence, a ubiquitous and important process found in many FPs and FP-based biosensors.[7−12] Studying excited state structural dynamics of this biochemical event in the presence and absence of the biotarget/analyte Ca^{2+} should therefore shed crucial light on the Ca^{2+}-sensing mechanism, which will help to pinpoint functional structural motifs and key pathways from the bottom up, develop protein engineering strategies, and further improve the green excitation ratiometric indicators to advance life sciences (Scheme 1).

To achieve this goal, we implement femtosecond stimulated Raman spectroscopy (FSRS), a powerful structural dynamics technique with simultaneously high spectral and temporal resolutions.[13−15] We track reactant species from the electronic ground (A in S_0) to excited state (A* in S_1), followed by ESPT barrier crossing toward the transient product species (I* state). This powerful experimental methodology yields high-quality vibrational spectra free from background fluorescence and also permits rapid collection of real-time vibrational spectra on the femtosecond (10^{-15} s, fs) to picosecond (10^{-12} s, ps) time scale of molecular species during photochemical reactions in solution.[14,16−19] Recently, we have used FSRS in the mixed time-frequency domain to study two Ca^{2+} biosensors, the blue-green emission ratiometric GEM-GECO1[11,20] and the green

Received: February 8, 2017
Revised: March 16, 2017
Published: March 22, 2017

DOI: 10.1021/acs.jpcb.7b01269
J. Phys. Chem. B XXXX, XXX, XXX−XXX

Scheme 1. Discovery Loop of the Functional Fluorescent Protein-based Biosensors

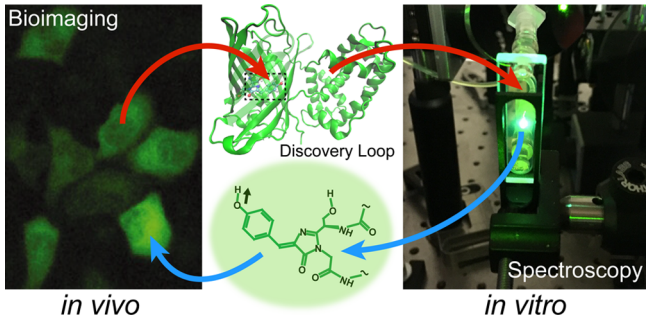

intensiometric G-GECO1.1,[12,21] which lay the foundation for this work. Herein, we present the ultrafast Raman spectra of GEX-GECO1 that infer its working mechanism in contrast to other Ca^{2+} biosensors, based on vibrational marker bands that track the ESPT pathways and different energy relaxation processes in the electronic excited state. The experimental results are well corroborated by molecular dynamic simulations. Our present work delineates the covert photochemical reaction coordinates inside a newly developed calcium biosensor under physiological conditions.

MATERIALS AND METHODS

Biosensor Sample Preparation. The GEX-GECO1 protein for *in vitro* spectroscopy was prepared as previously reported.[11] In brief, *E. coli* DH10B cells were transformed with the pTorPE plasmid harboring His6-GEX-GECO1.[6] The transformed *E. coli* cells were placed on a nutrient agar plate supplemented with ampicillin and arabinose. Following overnight growth, the brightly fluorescent colonies were picked and used to inoculate 1 L of a modified terrific broth (20 g Lysogeny broth mix, 7 g yeast extract, 14 g tryptone, 2.2 g KH_2PO_4, 9.2 g K_2HPO_4, and 8 mL glycerol to reach pH = 7.2, sterilized). The culture was allowed to grow at 30 °C for 2 days. The cells from the culture were collected via centrifugation, resuspended in Tris-buffered saline (TBS) at pH = 7.4, and then lysed by French press. After centrifugation, the GEX-GECO1 protein in the clarified solution was purified using the Ni-NTA affinity chromatography, followed by buffer exchange to MOPS (3-(*N*-morpholino)propanesulfonic acid) buffer with either 10 mM EGTA (Ca^{2+}-free sample) or 10 mM Ca-EGTA (Ca^{2+}-bound sample) at pH = 7.2. The GEX-GECO1 sample solutions were characterized *in vitro* using steady-state UV/visible (UV/vis) and fluorescence spectroscopy. To prepare the biosamples for time-resolved FSRS measurements, the protein was concentrated for the OD value at 400 nm to be above 10/cm path length.[9,11]

Femtosecond Stimulated Raman Spectroscopy (FSRS). Our experimental FSRS setup was described in the prior reports.[11,21,22] Seeded by a mode-locked Ti:sapphire fs oscillator (Mantis-5), the regenerative laser amplifier (Legend Elite-USP-1K-HE, Coherent, Inc.) provides ~35 fs fundamental pulse with a center wavelength of ~800 nm, an average power of ~4 W, and a repetition rate of 1 kHz. About 2 W of the fundamental pulse is split three-ways that generates a narrowband ps Raman pump at 800 nm via a home-built grating-slit-based spectral filter, a broadband fs Raman probe via the sapphire-crystal-based supercontinuum white light generation (then selecting the long-wavelength part in reference to the Raman pump), and an fs actinic pump at 400 nm via the BBO-crystal-based second harmonic generation (with the average power attenuated to ~0.5 mW to initiate photochemistry). We estimated the instrument response time by measuring the optical Kerr effect (OKE) signal between the fs actinic pump and Raman probe pulses to be ~150 fs for a 1 mm-thick solution sample, such as the photoacid pyranine in water between two 1 mm-thick quartz windows (48-Q-1, Starna Cells).[22]

The time-resolved Stokes Raman spectra covering ca. 600—1800 cm^{-1} are collected in the electronic excited state for time delays up to ~650 ps after 400 nm photoexcitation, predominantly exciting the protonated chromophore species (see Figure 1 for the biosensor absorption profile). The sample

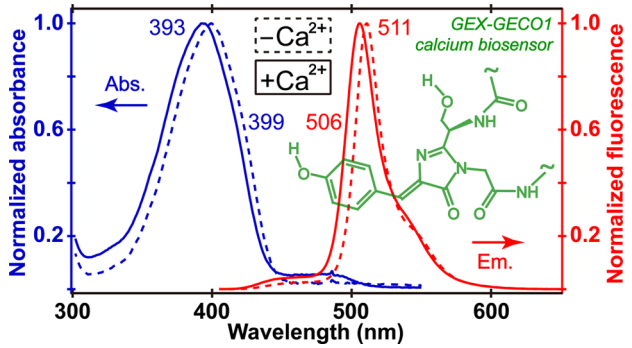

Figure 1. Electronic spectroscopy of GEX-GECO1 biosensor in aqueous buffer solution (pH = 7.2). The Ca^{2+}-free and bound samples are represented by dashed and solid traces, respectively. Normalized absorption and emission (λ_{ex} = 400 nm) spectra are shown against the left (blue) and right (red) vertical axes. The SYG chromophore structure (green) is depicted in the inset.

concentration is adjusted to OD ≈ 1/mm at 400 nm, and the protein sample is constantly flowing inside a quartz cell during the excited state FSRS measurements to avoid laser-induced thermal effects and/or potential photodegradation of biomolecules in solution.[9,11] The biosensor samples remain in a clear buffer solution, and are checked before and after each time-resolved excited state FSRS measurement to display no significant UV/vis absorption spectral changes (typically <5%) to ensure sample integrity (see Figure 1 for example). The related fs transient absorption measurements and corroborating results are described in the Supporting Information.

Notably, the FSRS spectral baseline drawing procedures for background subtraction have been established and extensively discussed in our previous reports,[9,11,12,21] and the prominent S_1 vibrational peaks analyzed and presented here (see Figures 2—6 below) are largely insensitive to the broad and featureless polynomial baselines. In addition, the systematic Gaussian-profile fits to the array of evolving vibrational peaks act as a noise filter and yield reliable experimental data on peak intensity, frequency, and width as a function of time delay following the actinic pump. In other words, the consistent and comparative aspects of the FSRS studies on FPs since inception have substantiated the technical efficacy and robustness of retrieving and analyzing the time-resolved Raman bands from many FP chromophores, which help elucidate the underlying ESPT reaction coordinates in dynamic protein pockets with compelling similarities and differences.

Molecular Dynamics (MD) Simulations. For the Ca^{2+}-free GEX-GECO1 biosensor without a currently available

DOI: 10.1021/acs.jpcb.7b01269
J. Phys. Chem. B XXXX, XXX, XXX−XXX

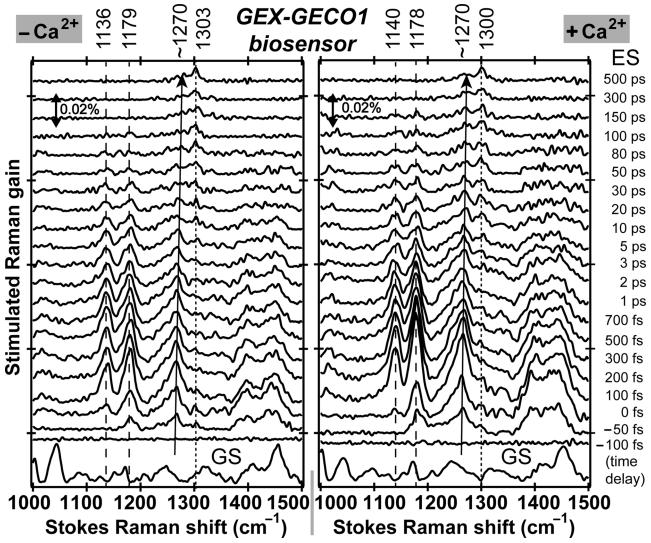

Figure 2. Time-resolved excited-state FSRS data of the Ca^{2+}-free and bound GEX-GECO1 biosensors following femtosecond 400 nm photoexcitation. The Raman pump is at 800 nm. The buffer and baseline-subtracted S_0 spectrum is plotted at the bottom. The S_0-subtracted S_1 vibrational modes evolving as a function of time (listed on the right) are highlighted by dashed lines. The frequency blueshift of the ~1270 cm^{-1} band is indicated by the upward curved arrow. The magnitude of the stimulated Raman gain of 0.02% is shown by the double-arrowed vertical line on the top left corner.

crystal structure, we used the Ca^{2+}-free GCaMP2 (PDB ID 3EKJ)[23] structure as a starting point and patched the M13 peptide from the Ca^{2+}-bound GCaMP2 (PDB ID 3EVR)[24] as well as the Ca^{2+}-free calmodulin (PDB ID 1CFD).[11,25] The initial coordinates of the Ca^{2+}-bound GEX-GECO1 biosensor are based on the Ca^{2+}-bound GCaMP2 (see below). Following published protein sequences, the GEX-GECO1-specific mutations in both protein chimera systems[6] are made using the Swiss PDB viewer.[26] The detailed MD simulation methodology for the Ca^{2+}-free case has been elaborated in our previous work.[11] The current force field for calcium ions is built using MCPB (Metal Center Parameter Builder) in AmberTools16.[27]

After 10 ns MD simulations, we plot the potential energy of the entire system as a function of time to verify the equilibrium state reached. In the Ca^{2+}-bound biosensor, the locations of calcium ions are closely examined to ensure that the coordinate bonds formed between calcium ions and surrounding residues are persistent. When compared with the starting point, i.e., the Ca^{2+}-bound GCaMP2, our simulation yields 0.853 Å root-mean-square (RMS) coordinate errors for 411 residues, indicating that the simulated structures are reliable at thermal equilibrium.[28] Note that the residues we count do not include the first 37 residues that are random coil (not typically reported in crystal structures) while the embedded chromophore is practically counted as one residue.

Because water molecules are not conserved in our simulations, after the system reaches thermal equilibrium, we calculate the distance between the O atom of the chromophore hydroxyl group of the tyrosine moiety and the O atom of the side chain hydroxyl of Ser118 (the first adjacent residue along the proton transfer chain) for 2500 random configurations which are spread throughout the simulation trajectory to ensure sufficient statistical sampling. We plot the distance distribution (with a 0.2 Å shifting window, see below for details) in both the Ca^{2+}-free and bound biosensor systems for direct comparison. Notably, the equilibrium MD simulations are sufficiently suitable to expose key structural constraints and potential tertiary interactions for the ultrafast ESPT reaction pathway(s) of the protein biosensor chromophore before and after Ca^{2+} binding, because the chromophore and its local environment should largely retain their atomic configurations starting from the photoexcitation time zero and in the Franck–Condon (FC) region.[9,11]

RESULTS AND DISCUSSION

Optical Characterization by Steady-State Electronic Spectroscopy. The electronic absorption and emission spectra of GEX-GECO1 (Figure 1) show that the Ca^{2+}-free biosensor has a dominant absorption peak at 399 nm, which corresponds to its protonated A state. Upon Ca^{2+} binding, the absorption peak blueshifts to 393 nm with a shoulder around 480 nm, indicating that most of the embedded Ser-Tyr-Gly (SYG) chromophore remains in the A state at thermal equilibrium. This leads to a small change of its fluorescence in one detection channel with ~480 nm excitation of the deprotonated (B) form in comparison to the intensiometric FP-based Ca^{2+} biosensors like GCaMP3.[6] However, two imaging channels with ~400 and 450 nm excitation can take full advantage of the fluorescence contrast afforded by GEX-GECO1. It effectively enables the ratiometric imaging and better quantification of the Ca^{2+} concentration for biomedical applications, also correcting common experimental variations such as photobleaching and cell motion. This specific attribute makes GEX-GECO1 a powerful biosensor for visualizing Ca^{2+} signaling events. Moreover, the 511 nm emission blueshifts to 506 nm in the Ca^{2+}-bound state. Both frequency blueshifts of the absorption and emission peaks indicate that the energy gap between the S_0 and S_1 state of this biosensor is increased with Ca^{2+}, whereas this trend is less significant in the G-GECO1.1 biosensor (emission peak 514 → 512 nm upon Ca^{2+} binding).[21]

Time-Resolved Raman Peaks Capture Molecular Movies with Chemical Bond Precision. The electronic spectroscopy of GEX-GECO1 biosensor at equilibrium conditions confirms the stationary fluorescence change of FP chromophore in response to Ca^{2+} binding events at the nearby calmodulin (CaM) domain. Starting from the equilibrated protein biosensors in solution, we collect the time-resolved FSRS data after 400 nm photoexcitation to elucidate intrinsic ESPT pathways during the nonequilibrium structural dynamics events mainly involving the chromophore, which lead to the characteristic fluorescence of the overall protein biosensor for bioimaging. Figure 2 shows the excited-state FSRS data for both the Ca^{2+}-free and bound GEX-GECO1 stacked as a function of time delay between the preceding actinic pump and the Raman probe, both fs pulses. A similar pattern of transient Raman peak dynamics shows that the chromophore A* modes rise at photoexcitation time zero and then decay with new peaks emerging near 1300 cm^{-1}, which are attributed to the aforementioned I* state. We note that various experimental conditions including the sample concentration, laser fluctuation, beam overlap, mode electric polarizability, resonance conditions may cause some differences in the observed peak intensity, so the spectral data analysis is performed for each sample individually to obtain accurate kinetics information for subsequent comparison. In addition, the choice of an 800 nm Raman pump pulse is suitable for tracking chromophore motions during this type of photochemical reactions[9,11,20,21]

DOI: 10.1021/acs.jpcb.7b01269
J. Phys. Chem. B XXXX, XXX, XXX–XXX

because the transient Raman peaks are selectively enhanced via the common broad excited-state absorption peak near 900 nm,[9] providing sufficient signal-to-noise ratio to dissect the pertaining ESPT pathway(s).

Primary structural events of the embedded chromophores within the first few ps after photoexcitation exhibit marked differences between biosensors before and after Ca^{2+} binding, which in turn govern their distinct fluorescence properties. Relevant atomic motions underlie the biosensor color change from green to blue and/or the intensity variation. Our previous studies show that the 1180 cm^{-1} mode (ring-H and bridge C−H rocking motion) tracks ESPT.[11,21] For GEX-GECO1, the A* mode intensity decay for both biosensors is plotted in Figure 3a

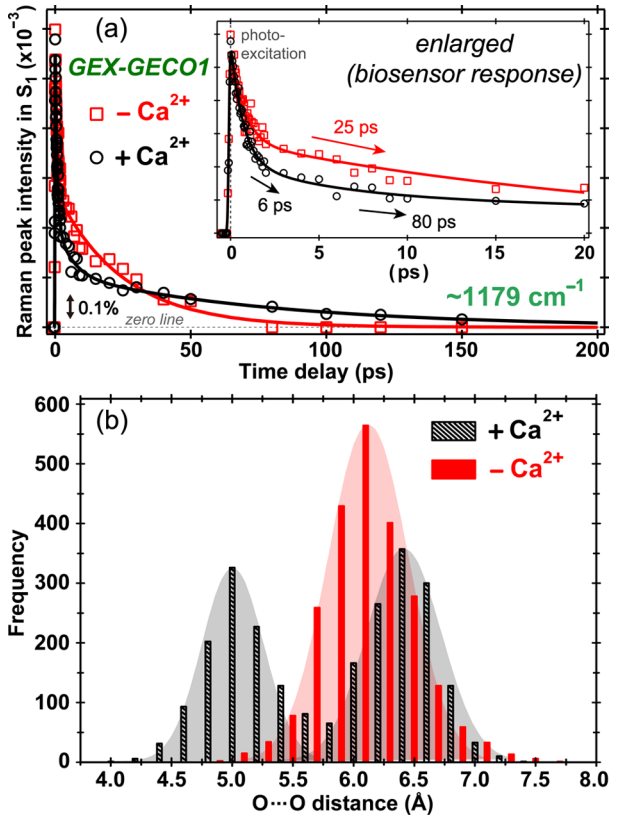

Figure 3. Time-resolved excited-state vibrational dynamics of GEX-GECO1 and structural basis. (a) Normalized intensity plot of the ~1179 cm^{-1} modes in the Ca^{2+}-free (red) and bound (black) biosensor within 200 ps. The inset shows an enlarged plot up to 20 ps after 400 nm photoexcitation. (b) Distribution of the O···O distance between the chromophore phenolic hydroxyl and Ser118 side chain. The distributions are shown using a histogram with 0.2 Å interval for the Ca^{2+}-free (red) and bound (black) biosensors, respectively, highlighted by shades with the corresponding colors.

starting from 400 nm photoexcitation. The Ca^{2+}-free sample shows a double-exponential decay with time constants of ~700 fs (55%) and 25 ps (45%), while the Ca^{2+}-bound sample shows a triple-exponential decay with time constants of ~600 fs (65%), 6 ps (18%), and 80 ps (17%). The comparison of the fits with double and triple-exponential decay for the 1178 cm^{-1} mode in the Ca^{2+}-bound biosensor (Figure S1, Supporting Information) clearly confirms that triple exponentials are required for a satisfactory fit of the mode intensity dynamics following electronic excitation. These results indicate that the Ca^{2+}-free biosensor has one ESPT channel with a 25 ps time constant, whereas two ESPT channels exist in the Ca^{2+}-bound biosensor with time constants of ~6 and 80 ps (see additional text, Supporting Information). Notably, for the initial sub-ps decay component which reflects the wavepacket dynamics moving out of the FC region after 400 nm photoexcitation, it weighs more in the Ca^{2+}-bound (65%) than the Ca^{2+}-free case (55%). This may be due to the fact that the Ca^{2+}-bound biosensor has more ESPT channels as a result of structural heterogeneity regarding the A* subpopulations and local H-bonding configurations around the chromophore.

The I* marker band at ~1300 cm^{-1} rises at later time (Figure 2), and its dynamics corroborate the ESPT time scales (Figure S2, Supporting Information). In the Ca^{2+}-free (bound) state, the mode intensity shows a decay-rise-decay pattern with ~500 (600) fs, 24 (15) ps, and 2.0 (1.3) ns time constants. The first decay component of 500−600 fs reflects the departure from the FC region as resonance Raman conditions change for the A* species in this spectral region. It is tempting to assign the 1300 cm^{-1} mode at early time to the directly excited deprotonated chromophore, however, two reasons refute this assignment. First, the SYG chromophore is predominantly protonated in the ground state (Figure 1) with no clear deprotonated population (B state). Second, the B state shows negligible absorption at 400 nm, our photoexcitation wavelength. Therefore, the initial peak decay in this region is likely associated with the small-scale, coherent proton motions starting from FC region of A* state where electron and proton motions are strongly coupled.[11,20,22,29] The second rise component of the ~1300 cm^{-1} mode tracks the ESPT reaction and accumulation of I* species. For the Ca^{2+}-free biosensor, the rise time constant of 24 ps matches the aforementioned main ps decay (25 ps) of the 1180 cm^{-1} mode (Figure 3a). After Ca^{2+} binding, the rise time constant of 15 ps matches the weighted average of ESPT time constants (6 and 80 ps) starting from time zero, which cannot be distinguished at this spectral location due to lower signal intensity and the overlap of I* and A* peaks. The third decay is shorter than typical fluorescence lifetime (~4 ns) of the I* state,[7,9,30] suggesting that other nonradiative energy relaxation or fluorescence quenching pathways exist in the biosensor which may contribute to its relatively low quantum yield of ~0.2.[6]

Key Structural Constraints from Molecular Dynamics Simulations. Due to the lack of crystal structures of the Ca^{2+}-free/bound GEX-GECO1, we perform complementary molecular dynamics (MD) simulations on equilibrium structures for both protein biosensors using Amber 12 software package[31] to understand the relationship between structure and dynamics of proton transfer (see Materials and Methods Section above). We expect that structural constraints around the chromophore, particularly at the proton dissociation site, play an essential role determining the ESPT reaction pathways. Since water molecules are not conserved in location, we calculate the distance between the O atoms of the chromophore phenolic hydroxyl and the Ser118 side chain, which is an integral part of the functional ESPT chain.[6,11] We plot the intermolecular distance distribution in the Ca^{2+}-free and bound systems in Figure 3b. In the Ca^{2+}-free case, the O···O distance fluctuates at thermal equilibrium but is largely concentrated around 6 Å during the entire simulation (Figure 4a). This distance is much longer than a typical H-bond so intervening water molecules are expected to act as a bridge. We suggest that the serine residue adopts one main conformation because the open β-barrel with large solvent access enables sufficient averaging

DOI: 10.1021/acs.jpcb.7b01269
J. Phys. Chem. B XXXX, XXX, XXX−XXX

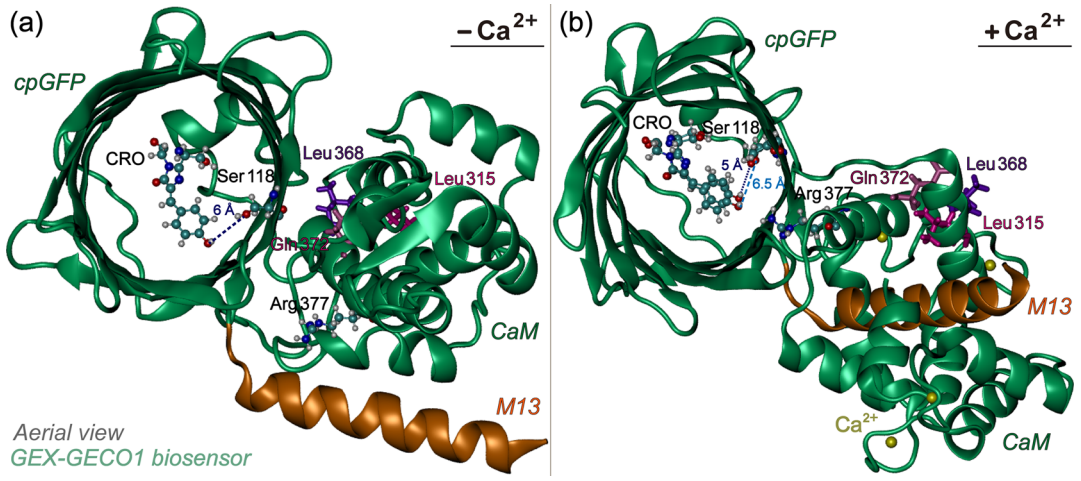

Figure 4. Snapshot structures of the (a) Ca^{2+}-free and (b) Ca^{2+}-bound GEX-GECO1 biosensors from MD simulations. The M13 peptide as the calmodulin (CaM) binding client is shown in orange, and the dramatic difference between its location in reference to the CaM unit (shown in green) upon Ca^{2+} binding is notable. The GEX-specific residues (Leu315, Leu368, and Gln372) and the interfacial Arg377 are color labeled. The typical O···O distances, 6 Å in (a) and 5, 6.5 Å overlaid in (b), between the chromophore phenolic hydroxyl and Ser118 side chain hydroxyl associated with the characteristic subpopulations are denoted inside the cpGFP β-barrel (shown in green on the left side), respectively. The four Ca^{2+} ions bound to CaM are shown in yellow spheres in (b). The top portion of the cpGFP is partially removed to better show the chromophore (CRO).

when compared to the wild-type (wt)GFP case.[32] We correlate this conformational state to the observed ESPT time constant from the FSRS data reported here, 25 ps, which is much longer than that in wtGFP (ca. 5 ps) wherein the key adjacent water molecule along the ESPT chain is largely conserved.[9,33,34]

Upon Ca^{2+} binding, the O···O distance exhibits distinct fluctuations within the same simulation window, and its distribution (see Figures 3b and 4b) suggests the existence of two major conformations of the biosensor chromophore pocket. One of the conformations has a shorter O(CRO)···O(Ser118) distance around 5 Å, indicating a "tight" H-bonding along the proton transfer pathway (see Figure 4b for depiction, blue dotted line). This intermolecular distance is similar to the O(CRO)···O(Ser205) case (4.3 Å) in a wtGFP crystallographic structure (PDB ID 1EMB),[32] and the associated ESPT time constant for GEX-GECO1 from the time-resolved FSRS data is ~6 ps (see Figure 3a). The other O···O distance cluster, ~ 6.5 Å, corresponds to a relatively "loose" H-bonding environment around the chromophore (see Figure 4b, cyan dashed line). Notably, previous all-atom explicit MD simulations on wtGFP[35] showed two conformations of Ser205, one of which prevents proton transfer. In the Ca^{2+}-bound GEX-GECO1, the β-barrel is not as conserved as wtGFP and the M13-client-induced opening still allows solvent exposure (Figure 4b), which could help form a different ESPT pathway that exhibits a longer ESPT time constant of ~80 ps.

The underlying cause for this observed ESPT variation originates from the protein structural change due to Ca^{2+} binding. In the absence of Ca^{2+}, the extended CaM domain is away from the circularly permuted (cp)GFP β-barrel opening (Figure 4a), so the chromophore is largely free to search for its global minimum equilibrium structure facilitated by solvation events.[36] This leads to a dominant chromophore local environment with its characteristic ESPT network particularly involving H-bonding. However, upon Ca^{2+} binding, the compressed CaM unit approaches the FP β-barrel opening and the positively charged interfacial residues like Arg377 are pushed toward the cpGFP pocket (Figure 4b).[11,21] The modified electrostatic interaction and particularly H-bonding effectively confine the chromophore environment and reduce the solvent exposure, so the chromophore and its surrounding residues may become trapped in their local minima with multiple configurations. In this case, two ESPT pathways coexist inside the Ca^{2+}-bound biosensor: one is faster (slower) than the Ca^{2+}-free case likely due to closer (farther) distance between the proton donor and acceptor (Figure 4). We consider that the slower, ~ 80 ps ESPT route starts from the mostly protonated chromophore subpopulation in S_0 that corresponds to the absorption peak at 393 nm (see Figure 1), which is blueshifted from the Ca^{2+}-free biosensor absorption peak at 399 nm.

Further Insights on ESPT and Vibrational Cooling from Intensity and Frequency Dynamics of the Chromophore Marker Bands. The ~1265 cm^{-1} mode is associated with the chromophore phenolic C−O stretch, which exhibits only decay behavior with no rise dynamics in either the Ca^{2+}-free or bound biosensor (Figure 5). This marker band

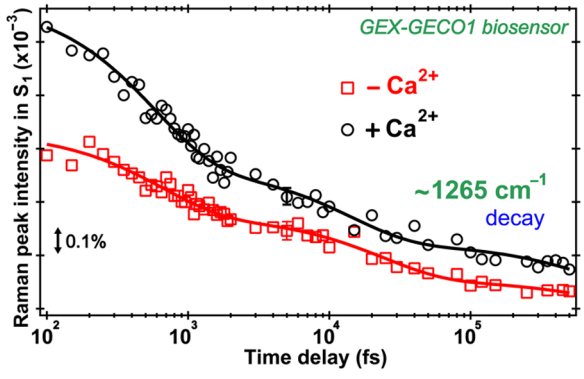

Figure 5. Kinetic intensity plot of the ~1265 cm^{-1} mode in the Ca^{2+}-free (red) and bound (black) GEX-GECO1 after 400 nm photoexcitation. The time delay axis in the logarithmic scale highlights the multiexponential nature of the decay least-squares fit (solid curves) between 100 fs and 500 ps. The representative error bars are shown for data points at 5 ps. For better comparison, the Ca^{2+}-bound data points are vertically offset by +0.05%.

DOI: 10.1021/acs.jpcb.7b01269
J. Phys. Chem. B XXXX, XXX, XXX−XXX

shows a triple-exponential decay with time constants of 630 fs (53%), 24 ps (33%), 830 ps (14%) for the Ca^{2+}-free GEX-GECO1 biosensor, and 600 fs (61%), 14 ps (23%), 740 ps (16%) for the Ca^{2+}-bound case. The continuous decay pattern indicates that this is an A* mode, and it does not diminish completely within our detection time window (~650 ps). The first time constant of ~600 fs results from the FC dynamics and is related to initial movement of the embedded chromophore that typically involve collective ring skeletal motions and small-scale proton motions.[11,20,22] The 24 ps decay of the Ca^{2+}-free case matches the 25 ps decay in the ~1180 cm^{-1} mode, corroborating the ESPT reaction coordinate. The 14 ps component in the Ca^{2+}-bound case reflects the ensemble average of two time constants (~6 and 80 ps) in the 1180 cm^{-1} mode (see Figure 3a), which cannot be clearly resolved due to spectral overlap between the A* peaks from slightly different molecular configurations (Figures 3b and 4b, see overlaid chromophore structures in the latter). The 700—800 ps time constant could arise from other radiative and/or nonradiative relaxation pathways from the remaining A* populations.[11,37]

Notably, the long-time dynamics of the 1265 cm^{-1} mode differ from the 1180 and 1300 cm^{-1} modes. Several factors contribute: A* or I* modes, the pertaining atomic motions (e.g., different mode sensitivity to structural events), contributions from various conformational states, and mode electric polarizability, etc.[11,17,22,38] It is imperative to interpret spectral observables in the context of all the vibrational marker bands, and correlate their time constants to gain a more complete picture of the excited state potential energy surface. For instance, the 1180 cm^{-1} peak decays away on the hundreds of ps time scale (Figures 2 and 3a) and reports on ESPT, mainly because it is associated with the A* population that undergoes ESPT while its corresponding normal mode (bridge-H and phenolic ring-H rocking, plus phenolic COH rocking motions)[11,21] is preresonantly enhanced in S_1 by the 800 nm Raman pump pulse. In contrast, the 1265 cm^{-1} peak consists of the phenolic C—O stretch and besides probing ESPT, it could display more sensitivity to the A* population that does not undergo ESPT. Therefore, we not only observed a further decay of the mode intensity (see Figure 5) beyond the ESPT time scales, but also recorded a frequency blueshift (Figure 6). Interestingly, the 1300 cm^{-1} mode (Figure S2, Supporting Information) does not show a noticeable blueshift so we may need to tune the Raman pump toward the blue region to specifically enhance I* features[12,21] and examine the vibrational cooling dynamics after the ESPT barrier crossing.[39−41]

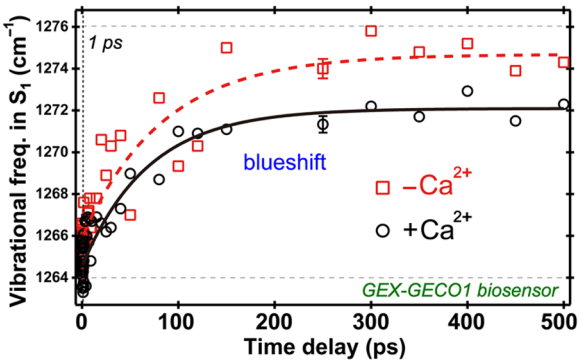

Figure 6. Excited-state vibrational frequency shift of the ~1265 cm^{-1} mode in the Ca^{2+}-free (red squares) and bound (black circles) GEX-GECO1 biosensor up to 500 ps after 400 nm photoexcitation. The starting time delay for the single-exponential fit is noted by the vertical dotted line at 1 ps. Representative error bars are shown for the FSRS data points at 250 ps.

The marker band at ~1265 cm^{-1} provides further insights into energy dissipation pathways of the A* population(s). Notably, this mode blueshifts to ~1275 cm^{-1} with a dominant time constant of 70 and 90 ps in the Ca^{2+}-free and bound biosensor (Figure 6), respectively, after a dwell of ~1 ps which is a "bifurcation" point for ESPT reaction (to I*) and further vibrational relaxation (to lower A*). By 1 ps, the system is out of the FC region with its internal energy largely distributed among vibrational modes so the interaction between the chromophore and protein environment plays a significant role.[42,43] This observation reflects vibrational cooling to the surroundings for A* species beyond ESPT, and the chromophore could undergo large-scale structural changes to dissipate the excess energy from photoexcitation. For the Ca^{2+}-free biosensor, the chromophore has more free space to move because of the β-barrel opening and a distant CaM unit (Figure 4a), which allow the GFP local environment to rearrange faster, also exhibiting a larger blueshift of mode frequency (Figure 6). In the Ca^{2+}-bound biosensor with overall compact (i.e., ~ 15 ps average ESPT rate retrieved from the I* mode rise dynamics, faster than 24 ps of the Ca^{2+}-free case) and some tighter H-bonding interactions, the photoexcited chromophore (active site) and its surrounding residues need more energy to rearrange configurations, resulting in longer time for vibrational cooling and less frequency change.

This result is significant for three reasons: (1) the transient Raman mode frequency dynamics differ from intensity dynamics insofar as the ~10 cm^{-1} frequency blueshift is more sensitive to vibrational relaxation/cooling within the A* state; (2) this result reveals the energy relaxation rate of the A* subpopulation that does not undergo ESPT; and (3) a similar A* mode blueshift was not seen for the SYG chromophore in GEM-GECO1 or a related TYG chromophore in G-GECO1.1 with the same Raman pump wavelength of 800 nm.[11,21] In particular, the 1275 cm^{-1} A* mode in both the Ca^{2+}-free and bound GEX-GECO1 is a unique feature of this biosensor beyond the main ESPT event. One explanation is that the interfacial Arg377 and other GEX-specific residues[6] like Gln372, Leu368, and Leu315 provide distinct short and long-range interactions to modify the potential energy surface of the embedded SYG chromophore (see Figure 4). This leads to the resonance Raman enhancement for A* species that evolve in parallel with the ESPT reaction.

Furthermore, we recently identified a single Pro377Arg (P377R) mutation that converts the ratiometric GEM-GECO1 into an excitation ratiometric Ca^{2+} biosensor with similar electronic absorption and emission to GEX-GECO1 (Figure S3, Supporting Information). This substantiates the importance of an interfacial arginine residue, and the FSRS results of the P377R mutant biosensor have been reported.[44] The comparison between the two excitation ratiometric biosensors is telling: the common SYG chromophore conformational heterogeneity is similar in exhibiting a bimodal distribution of O···O distances between the chromophore phenolic hydroxyl group and a nearby proton acceptor like the serine side chain hydroxyl, however, the much faster 6 ps ESPT time constant retrieved from the transient Raman marker band intensity dynamics (Figure 3a) of GEX-GECO1 (versus the corresponding 16 ps component in GEM-GECO1-P377R)[44] reveals an important working principle for a fast Ca^{2+} biosensor to be the

DOI: 10.1021/acs.jpcb.7b01269
J. Phys. Chem. B XXXX, XXX, XXX−XXX

availability of a compact H-bonding chain between the chromophore and the surrounding protein matrix. In other words, the secondary structure and tertiary interaction in the vicinity of the chromophore pocket, i.e., the active site of the FP biosensor, dictate the photochemical reaction pathways on ultrafast time scales (observable by excited-state FSRS), ultimately leading to the characteristic fluorescence properties. Moreover, even though the GEM-GECO1-P377R biosensor does not achieve an optimized H-bonding network to support a more deprotonated chromophore subpopulation to exhibit a faster ESPT rate, it represents a proof of principle study that showcases the power of site-specific mutagenesis with mechanistic insights from spectroscopy to improve a certain functionality of the system.

The formation of an extended H-bonding network involving the CaM residues may explain why GEX-GECO1 among all GECOs has the fastest response to Ca^{2+}.[6] The 6 ps ESPT rate is similar to ∼5 ps in wtGFP with the closed β-barrel,[9] fewer internal water molecules, and a better protected SYG chromophore. This specific subpopulation of the Ca^{2+}-bound GEX-GECO1 with "tighter" H-bonding interactions (Figures 3b and 4b), reminiscent of the protected wtGFP interior, is unique among all the GECOs and may serve to effectively lower the enthalpy of the protein matrix particularly around the chromophore and help drive the biosensor rapidly to equilibrium upon Ca^{2+} binding on the macroscopic time scale. This improved biosensor attribute will be highly desirable for *in vivo* bioimaging targets from cancer metastasis to brain activities.

CONCLUDING REMARKS

We have revealed the working mechanism via functional variation of the excited state proton transfer (ESPT) pathways and rates in an emergent excitation ratiometric biosensor GEX-GECO1 upon Ca^{2+} binding. A sophisticated ultrafast stimulated Raman methodology has been developed and implemented for this investigation. Besides the critical importance of FPs across modern science and engineering fields, ESPT reaction occurs through an intricate H-bonding network in native chemical and biological environment so FPs afford an almost idealistic system for the fundamental study on this ubiquitous process (see Scheme 1). The structural dynamics findings of this excitation ratiometric FP-based biosensor are thus not limited to just one specific system, instead they are useful and applicable to a broad community of researchers and developers interested in harnessing the power of H-bonding interactions, chromophore−protein matrix interplay, as well as site-specific mutagenesis to tune and control electron and nuclear motions which intrinsically govern the overall macroscopic functions of those molecular systems.

Notably, a number of vibrational marker bands between 1100−1350 cm^{-1} provide a wealth of previously unavailable information about GEX-GECO1 on the ultrafast time scales with high spatial sensitivity at the chemical bond level. The Ca^{2+}-bound biosensor consists of two major populations which exhibit distinct chromophore environments with different ESPT capabilities (∼6 and 80 ps time constants), while the Ca^{2+}-free biosensor shows one dominant population (∼25 ps ESPT time constant), supported by systematic nanosecond MD simulations. The structural difference between Ca^{2+}-free and bound GEX-GECO1 may be the cause of it exhibiting the fastest Ca^{2+} response among all GECOs. The blueshift of the ∼1265 cm^{-1} mode on the tens of ps time scale uncovers hitherto hidden vibrational cooling pathways inside the protein pocket for chromophore species that does not undergo ESPT. Based on these newly acquired structural dynamics findings on molecular time scales, we expect that strategically tuning the chromophore environment to form additional and stronger H-bonds can accelerate the Ca^{2+} response time and the overall ESPT reaction rate thus help to develop more efficient ion sensors for bioimaging applications.

ASSOCIATED CONTENT

Supporting Information

The Supporting Information is available free of charge on the ACS Publications website at DOI: 10.1021/acs.jpcb.7b01269.

Femtosecond transient absorption, vibrational insights into the optical properties of GEX-GECO1 biosensor, Figures S1−S3, and additional references with full authorships (PDF)

AUTHOR INFORMATION

Corresponding Author

*E-mail: Chong.Fang@oregonstate.edu; Phone: 541-737-6704.

ORCID

Longteng Tang: 0000-0001-9316-188X

Chong Fang: 0000-0002-8879-1825

Present Addresses

[§]School of Physical Science and Technology, ShanghaiTech University, Pudong, Shanghai 201210, P. R. China.

[⊥]MIT Media Lab, Massachusetts Institute of Technology, Cambridge, MA 02139, United States.

Notes

The authors declare no competing financial interest.

ACKNOWLEDGMENTS

We thank Dr. Fangyuan Han for Igor programming and Breland Oscar for helpful discussions. This work was supported in part by the U.S. NSF CAREER grant (CHE-1455353) to C.F., and Natural Sciences and Engineering Research Council of Canada and Canadian Institutes of Health Research grants to R.E.C.

REFERENCES

(1) Prevarskaya, N.; Skryma, R.; Shuba, Y. Calcium in Tumour Metastasis: New Roles for Known Actors. *Nat. Rev. Cancer* **2011**, *11*, 609−618.

(2) Grienberger, C.; Konnerth, A. Imaging Calcium in Neurons. *Neuron* **2012**, *73*, 862−885.

(3) Chalfie, M.; Tu, Y.; Euskirchen, G.; Ward, W. W.; Prasher, D. C. Green Fluorescent Protein as a Marker for Gene Expression. *Science* **1994**, *263*, 802−805.

(4) Tsien, R. Y. The Green Fluorescent Protein. *Annu. Rev. Biochem.* **1998**, *67*, 509−544.

(5) Newman, R. H.; Fosbrink, M. D.; Zhang, J. Genetically Encodable Fluorescent Biosensors for Tracking Signaling Dynamics in Living Cells. *Chem. Rev.* **2011**, *111*, 3614−3666.

(6) Zhao, Y.; Araki, S.; Wu, J.; Teramoto, T.; Chang, Y.-F.; Nakano, M.; Abdelfattah, A. S.; Fujiwara, M.; Ishihara, T.; Nagai, T.; et al. An Expanded Palette of Genetically Encoded Ca^{2+} Indicators. *Science* **2011**, *333*, 1888−1891.

(7) Chattoraj, M.; King, B. A.; Bublitz, G. U.; Boxer, S. G. Ultra-Fast Excited State Dynamics in Green Fluorescent Protein: Multiple States and Proton Transfer. *Proc. Natl. Acad. Sci. U. S. A.* **1996**, *93*, 8362−8367.

(8) Stoner-Ma, D.; Jaye, A. A.; Matousek, P.; Towrie, M.; Meech, S. R.; Tonge, P. J. Observation of Excited-State Proton Transfer in Green Fluorescent Proetin using Ultrafast Vibrational Spectroscopy. *J. Am. Chem. Soc.* **2005**, *127*, 2864−2865.
(9) Fang, C.; Frontiera, R. R.; Tran, R.; Mathies, R. A. Mapping GFP Structure Evolution during Proton Transfer with Femtosecond Raman Spectroscopy. *Nature* **2009**, *462*, 200−204.
(10) van Thor, J. J.; Lincoln, C. N.; Kellner, B.; Bourdakos, K. N.; Thompson, L. M.; Bearpark, M. J.; Champion, P. M.; Sage, J. T. Ultrafast Vibrational Dynamics of Parallel Excited State Proton Transfer Reactions in the Green Fluorescent Protein. *Vib. Spectrosc.* **2012**, *62*, 1−6.
(11) Oscar, B. G.; Liu, W.; Zhao, Y.; Tang, L.; Wang, Y.; Campbell, R. E.; Fang, C. Excited-State Structural Dynamics of a Dual-Emission Calmodulin-Green Fluorescent Protein Sensor for Calcium Ion Imaging. *Proc. Natl. Acad. Sci. U. S. A.* **2014**, *111*, 10191−10196.
(12) Tang, L.; Liu, W.; Wang, Y.; Zhu, L.; Han, F.; Fang, C. Ultrafast Structural Evolution and Chromophore Inhomogeneity inside a Green-Fluorescent-Protein-Based Ca^{2+} Biosensor. *J. Phys. Chem. Lett.* **2016**, *7*, 1225−1230.
(13) Yoshizawa, M.; Kurosawa, M. Femtosecond Time-Resolved Raman Spectroscopy Using Stimulated Raman Scattering. *Phys. Rev. A: At., Mol., Opt. Phys.* **1999**, *61*, 013808.
(14) McCamant, D. W.; Kukura, P.; Yoon, S.; Mathies, R. A. Femtosecond Broadband Stimulated Raman Spectroscopy: Apparatus and Methods. *Rev. Sci. Instrum.* **2004**, *75*, 4971−4980.
(15) Kukura, P.; McCamant, D. W.; Mathies, R. A. Femtosecond Stimulated Raman Spectroscopy. *Annu. Rev. Phys. Chem.* **2007**, *58*, 461−488.
(16) Weigel, A.; Dobryakov, A.; Klaumünzer, B.; Sajadi, M.; Saalfrank, P.; Ernsting, N. P. Femtosecond Stimulated Raman Spectroscopy of Flavin after Optical Excitation. *J. Phys. Chem. B* **2011**, *115*, 3656−3680.
(17) Frontiera, R. R.; Fang, C.; Dasgupta, J.; Mathies, R. A. Probing Structural Evolution along Multidimensional Reaction Coordinates with Femtosecond Stimulated Raman Spectroscopy. *Phys. Chem. Chem. Phys.* **2012**, *14*, 405−414.
(18) Kuramochi, H.; Takeuchi, S.; Tahara, T. Ultrafast Structural Evolution of Photoactive Yellow Protein Chromophore Revealed by Ultraviolet Resonance Femtosecond Stimulated Raman Spectroscopy. *J. Phys. Chem. Lett.* **2012**, *3*, 2025−2029.
(19) Hoffman, D. P.; Mathies, R. A. Femtosecond Stimulated Raman Exposes the Role of Vibrational Coherence in Condensed-Phase Photoreactivity. *Acc. Chem. Res.* **2016**, *49*, 616−625.
(20) Wang, Y.; Tang, L.; Liu, W.; Zhao, Y.; Oscar, B. G.; Campbell, R. E.; Fang, C. Excited State Structural Events of a Dual-Emission Fluorescent Protein Biosensor for Ca^{2+} Imaging Studied by Femtosecond Stimulated Raman Spectroscopy. *J. Phys. Chem. B* **2015**, *119*, 2204−2218.
(21) Tang, L.; Liu, W.; Wang, Y.; Zhao, Y.; Oscar, B. G.; Campbell, R. E.; Fang, C. Unraveling Ultrafast Photoinduced Proton Transfer Dynamics in a Fluorescent Protein Biosensor for Ca^{2+} Imaging. *Chem. - Eur. J.* **2015**, *21*, 6481−6490.
(22) Liu, W.; Han, F.; Smith, C.; Fang, C. Ultrafast Conformational Dynamics of Pyranine during Excited State Proton Transfer in Aqueous Solution Revealed by Femtosecond Stimulated Raman Spectroscopy. *J. Phys. Chem. B* **2012**, *116*, 10535−10550.
(23) Akerboom, J.; Rivera, J. D. V.; Guilbe, M. M. R.; Malavé, E. C. A.; Hernandez, H. H.; Tian, L.; Hires, S. A.; Marvin, J. S.; Looger, L. L.; Schreiter, E. R. Crystal Structures of the GCaMP Calcium Sensor Reveal the Mechanism of Fluorescence Signal Change and Aid Rational Design. *J. Biol. Chem.* **2009**, *284*, 6455−6464.
(24) Wang, Q.; Shui, B.; Kotlikoff, M. I.; Sondermann, H. Structural Basis for Calcium Sensing by GCaMP2. *Structure* **2008**, *16*, 1817−1827.
(25) Kuboniwa, H.; Tjandra, N.; Grzesiek, S.; Ren, H.; Klee, C. B.; Bax, A. Solution Structure of Calcium-Free Calmodulin. *Nat. Struct. Biol.* **1995**, *2*, 768−776.
(26) Guex, N.; Peitsch, M. C. SWISS-MODEL and the Swiss-PDB Viewer: An Environment for Comparative Protein Modeling. *Electrophoresis* **1997**, *18*, 2714−2723.
(27) Case, D. A.; Betz, R. M.; Botello-Smith, W.; Cerutti, D. S.; Cheatham, I.; Darden, T. A.; Duke, R. E.; Giese, T. J.; Gohlke, H.; Goetz, A. W.; et al. *AMBER 2016*; University of California: San Francisco, CA, 2016.
(28) Kufareva, I.; Abagyan, R. Methods of Protein Structure Comparison. In *Homology Modeling: Methods and Protocols*; Orry, W. A. J., Abagyan, R., Eds.; Humana Press: Totowa, NJ, 2012; Vol. *857*, pp 231−257.
(29) Westlake, B. C.; Brennaman, M. K.; Concepcion, J. J.; Paul, J. J.; Bettis, S. E.; Hampton, S. D.; Miller, S. A.; Lebedeva, N. V.; Forbes, M. D. E.; Moran, A. M.; et al. Concerted Electron-Proton Transfer in the Optical Excitation of Hydrogen-Bonded Dyes. *Proc. Natl. Acad. Sci. U. S. A.* **2011**, *108*, 8554−8558.
(30) Meech, S. R. Excited State Reactions in Fluorescent Proteins. *Chem. Soc. Rev.* **2009**, *38*, 2922−2934.
(31) Case, D. A.; Darden, T. A.; Cheatham, I.; Simmerling, C. L.; Wang, J.; Duke, R. E.; Luo, R.; Walker, R. C.; Zhang, W.; Merz, K. M.; et al. *AMBER 12*; University of California: San Francisco, CA, 2012.
(32) Brejc, K.; Sixma, T. K.; Kitts, P. A.; Kain, S. R.; Tsien, R. Y.; Ormö, M.; Remington, S. J. Structural Basis for Dual Excitation and Photoisomerization of the *Aequorea victoria* Green Fluorescent Protein. *Proc. Natl. Acad. Sci. U. S. A.* **1997**, *94*, 2306−2311.
(33) Zimmer, M. Green Fluorescent Protein (GFP): Applications, Structure, and Related Photophysical Behavior. *Chem. Rev.* **2002**, *102*, 759−781.
(34) Tonge, P. J.; Meech, S. R. Excited State Dynamics in the Green Fluorescent Protein. *J. Photochem. Photobiol., A* **2009**, *205*, 1−11.
(35) Simkovitch, R.; Huppert, A.; Huppert, D.; Remington, S. J.; Miller, Y. Proton Transfer in Wild-Type GFP and S205V Mutant Is Reduced by Conformational Changes of Residues in the Proton Wire. *J. Phys. Chem. B* **2013**, *117*, 11921−11931.
(36) Koretke, K. K.; Luthey-Schulten, Z.; Wolynes, P. G. Self-Consistently Optimized Energy Functions for Protein Structure Prediction by Molecular Dynamics. *Proc. Natl. Acad. Sci. U. S. A.* **1998**, *95*, 2932−2937.
(37) Kummer, A. D.; Wiehler, J.; Schüttrigkeit, T. A.; Berger, B. W.; Steipe, B.; Michel-Beyerle, M. E. Picosecond Time-Resolved Fluorescence from Blue-Emitting Chromophore Variants Y66F and Y66H of the Green Fluorescent Protein. *ChemBioChem* **2002**, *3*, 659−663.
(38) McHale, J. L. *Molecular Spectroscopy*; Prentice-Hall: Upper Saddle River, NJ, 1999.
(39) Lian, T.; Locke, B.; Kholodenko, Y.; Hochstrasser, R. M. Energy Flow from Solute to Solvent Probed by Femtosecond IR Spectroscopy: Malachite Green and Heme Protein Solutions. *J. Phys. Chem.* **1994**, *98*, 11648−11656.
(40) Kennis, J. T. M.; Larsen, D. S.; Stokkum, I. H. M. v.; Vengris, M.; Thor, J. J. v.; Grondelle, R. v. Uncovering the Hidden Ground State of Green Fluorescent Protein. *Proc. Natl. Acad. Sci. U. S. A.* **2004**, *101*, 17988−17993.
(41) Stoner-Ma, D.; Jaye, A. A.; Ronayne, K. L.; Nappa, J.; Meech, S. R.; Tonge, P. J. An Alternate Proton Acceptor for Excited-State Proton Transfer in Green Fluorescent Protein: Rewiring GFP. *J. Am. Chem. Soc.* **2008**, *130*, 1227−1235.
(42) Henry, E. R.; Eaton, W. A.; Hochstrasser, R. M. Molecular Dynamics Simulations of Cooling in Laser-Excited Heme Proteins. *Proc. Natl. Acad. Sci. U. S. A.* **1986**, *83*, 8982−8986.
(43) Mizutani, Y.; Kitagawa, T. Direct Observation of Cooling of Heme upon Photodissociation of Carbonmonoxy Myoglobin. *Science* **1997**, *278*, 443−446.
(44) Tachibana, S. R.; Tang, L.; Wang, Y.; Zhu, L.; Liu, W.; Fang, C. Tuning Calcium Biosensors with a Single-Site Mutation: Structural Dynamics Insights from Femtosecond Raman Spectroscopy. *Phys. Chem. Chem. Phys.* **2017**, *19*, 7138−7146.

DOI: 10.1021/acs.jpcb.7b01269
J. Phys. Chem. B XXXX, XXX, XXX−XXX